Sagan Summer School 2015:
GlobalPFE
A simple model for planetary population synthesis

Christoph Mordasini

PlanetsInTime Research Group, University of Bern, Switzerland

1. Introduction

At the 2015 Sagan Summer Workshop you will have the opportunity to experiment with a toy population synthesis model called GlobalPFE which stands for Global Planet Formation and Evolution model. It is based on the original Ida and Lin (2004) model, but it also includes elements of several other models like Alibert et al. (2005); Mordasini et al. (2009a); Dittkrist et al. (2014). Recent reviews of population synthesis methods are found in Benz et al. (2014) and Mordasini et al. (2015).

The basic idea behind the planetary population synthesis method (Figure 1) is that the observed diversity of extrasolar planets is due to a diversity in the initial conditions, i.e. the protoplanetary disks. While it is typically difficult to observe the process of planet formation directly, in a numerical model the link between the planets and the initial conditions can be established with so-called global planet formation models. They directly predict the final (potentially observable) properties of synthetic extrasolar planets based on the properties of their parent synthetic protoplanetary disk. These global models build on simplified results from detailed modeling of the key processes of planet formation, like accretion and migration. Thanks to them, the population-wide, statistical consequences of a physical model (e.g., for orbital migration) become clear and can be statistically compared with the observed population (e.g., the semi-major axis distribution). This means that first, theoretical models of a specific process can be put to the observational test (which is otherwise often difficult), and second that the full wealth of observational data (the entire statistical information coming from different observational techniques like radial velocities, transits, direct imaging, microlensing, ...) can be used to constrain theoretical planet formation models.

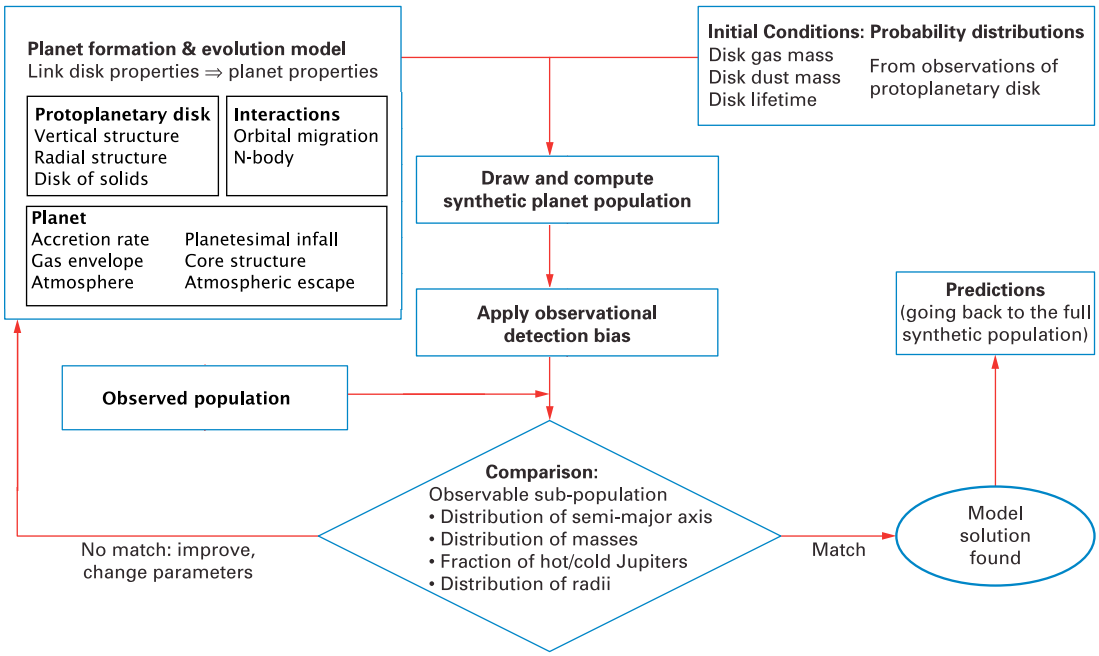

Fig. 1.— Elements and work flow of a planetary population synthesis framework.

The planet formation model considered here is based on the core accretion paradigm (Pollack et al. 1996) which states that giant planets form in a two-step process. First a critical solid core is built, which then triggers the accretion of the gaseous envelope. This happens in an evolving disk of gas and solids in which also other protoplanets grow, leading to dynamical interactions. The disk and the protoplanet exchange angular momentum, leading to orbital migration. Therefore, a global planet formation model must consider this minimal set of physical processes:

1. Structure and evolution of the protoplanetary disk
2. Accretion of solids / growth of the planetary solid core
3. Accretion of H/He / growth of the planetary gaseous envelope
4. Orbital migration
5. N-body interaction among (proto)planets

In this toy model we neglect the interactions of the concurrently growing protoplanets, but we model the other four processes by integrating numerically the temporal evolution of the planetary core mass, envelope mass, and semi-major axis, and we follow the evolution of the protoplanetary disk. The physical models used to describe these processes are described in the following sections.

2. Protoplanetary disk model

The disk model describes the evolution of the surface density of gas and solids. It also gives the temperature and vertical scale height. For the temperature T as a function of the distance r from the star, we simply assume as Ida and Lin (2004), a power law with

$$T(r) = 280\mathrm{K} \left(\frac{r}{1\mathrm{AU}}\right)^{p_T} \left(\frac{M_\star}{M_\odot}\right) \tag{1}$$

where $\mathrm{M}_\star$ is the mass of the star, and $p_T = -1/2$ for a passively irradiated disk. This simple presciption neglects the effect of viscous heating and does not include any temporal evolution, which is certainly an important limitation. The power law exponent can be set in the *paramsPFE.in* file (nominal value -1/2). It affects for example the Type I migration rate for some prescriptions, or the value of the vertical scale height and thus the mass when planets pass from Type I to Type II migration. The temperature is used to calculate the sound speed as

$$c_s(r) = \sqrt{\frac{k_\mathrm{B} T(r)}{\mu m_\mathrm{H}}} \tag{2}$$

where k_B is the Boltzmann constant, $\mu = 2.4$ the mean molecular mass, and m_H is the mass of a hydrogen atom. The vertical scale height is

$$H = c_s/\Omega \tag{3}$$

where the Keplerian orbital frequency is

$$\Omega = \sqrt{\frac{GM_\star}{r^3}}. \tag{4}$$

The gas surface density is assumed to consist of a sharp dropoff close to the star due to the magnetospheric cavity, a power-law in the main part, and an exponential decrease outside of a characteristic radius. This is inspired by the results of Lynden-Bell and Pringle (1974a) regarding the structure close to the star, and Andrews et al. (2010) for the outer part. The initial gas surface density is

$$\Sigma_\mathrm{g}(t=0,r) = \Sigma_{\mathrm{g},0} f_\mathrm{g} \left(\frac{r}{1\mathrm{AU}}\right)^{p_{\mathrm{g},0}} \exp\left[-\left(\frac{r}{R_\mathrm{out}}\right)^{2+p_{\mathrm{g},0}}\right] \left(1-\sqrt{\frac{r}{R_\mathrm{in}}}\right) \tag{5}$$

where $\Sigma_{\mathrm{g},0} = 2400$ g/cm^2 is the surface density in the MMSN (minimum-mass solar nebula model), f_g the scaling factor of the gas surface density (and thus initial disk gas mass), R_out the outer disk radius, R_in in inner radius, and $p_{\mathrm{g},0}$ the power law exponent. The quantities

$f_{\rm g}, R_{\rm out}$ and $R_{\rm in}$ are all initial conditions and Monte Carlo random variables in a population synthesis. The power law exponent is assumed to be $p_{\rm g} = -p_T - 3/2$ a relation that holds for strictly speaking only for viscously heated disk (thus this is not self-consistent). In the nominal case, we thus have $\Sigma_{\rm g} \propto r^{-1}$, which is similar to observations (Andrews et al. 2010). In the code it is however also possible to give $p_{\rm g}$ and p_T independently.

The initial surface density of solids is calculated as in Mordasini et al. (2009a) as

$$\Sigma_d(t=0,r) = f_{\rm D/G,\odot} 10^{\rm [Fe/H]} \eta_{\rm ice} \Sigma_{\rm g}(t=0,r) \tag{6}$$

where $f_{\rm D/G,\odot} = 0.0149$ is the dust-to-gas ratio (≈heavy element fraction) in the Sun (the value can be changed in the parameter file), [Fe/H] the metallicity (which is again a Monte Carlo variable) and $\eta_{\rm ice}$ reflects the increase of the surface density at the iceline. It is equal to 0.25 inside of the ice line, and 1 outside. The iceline corresponds to the distance where the temperature falls below 170 K.

2.1. Temporal evolution

In principle, the evolution of the gas disk should be calculated by solving the equation describing a viscous accretion disk including photoevaporation (e.g. Mordasini et al. 2015). In the simple GlobalPFE model we rather follow Ida and Lin (2004) and calculate

$$\dot{\Sigma}_{\rm g}(r) = -\frac{\Sigma_{\rm g}(r)}{\tau_{\rm disk}} + \dot{\Sigma}_{\rm wind} \tag{7}$$

The first term on the right side would lead to an exponential self-similar decay (due to viscous accretion onto the star), while the second one mimics the effects of photoevaporation leading to a shrinking of the disk. The characteristic disk timescale $\tau_{\rm disk}$ is another initial condition and Monte Carlo variable. $\dot{\Sigma}_{\rm wind}$ is assumed to be $10^{-7} M_\odot$/yr / (100 AU)^2 as a rough estimate. The evolution of the gas disk does not include the effect of the accretion onto the planet. In this sense, we do not conserve mass.

The surface density of solids decreases within the planet feeding zone according to the amount of mass that the planet accretes, assuming that the surface density is uniform within the feeding zone (Thommes et al. 2003), i.e.

$$\dot{\Sigma}_{\rm d} = -\frac{(3M_*)^{1/3}}{6\pi a_{\rm p}^2 B_L M_{\rm p}^{1/3}} \dot{M}_{\rm c} \tag{8}$$

where B_L is the width of the feeding zone in Hill spheres, $M_{\rm p}$ the planet mass, $a_{\rm p}$ its orbital semi-major axis, and $\dot{M}_{\rm c}$ the planet solid core accretion rate. Other effects that could modify the surface density of planetesimals, like drift, are neglected. Figure 2 shows the initial solid surface density for a 5 times MMSN disk (black line) and how a protoplanet growing in situ at about 7 AU "eats" into the disk by accreting planetesimals.

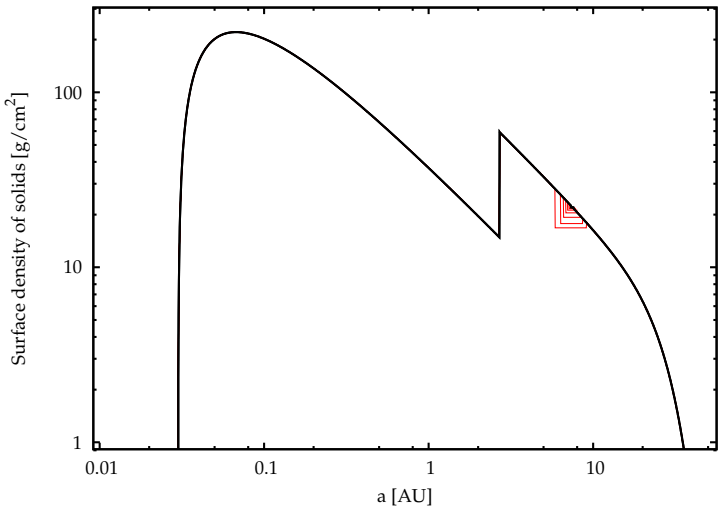

Fig. 2.— Solid surface density as a function of semi-major axis and time. The black line is the initial condition (nearly) while the red lines are later moments in time. The inner radius is 0.03 AU, the outer 30 AU.

The full width of the feeding zone is taken to be 12 Hill sphere radii where the Hill sphere radius is

$$R_H = \left(\frac{M_p}{3M_\star}\right)^{1/3} a_p \tag{9}$$

with total mass of the planet M_p as the sum of M_c the mass of the core and M_e the mass of the H/He envelope.

3. Accretion of planetesimals

The growth of the solid core with mass M_c is assumed to occur in the classical picture via the accretion of small background planetesimals. We use the same equation as Ida and Lin (2004), describing the accretion rate in the oligarchic growth regime. The random velocities of the planetesimals are raised by viscous stirring by the protoplanet, while they are damped

by gas drag (when the gas disk is still present). The accretion timescale in this regime is

$$\tau_{\rm c,gas} = 1.2 \times 10^5 \ {\rm yr} \left(\frac{\Sigma_{\rm d}}{10 \ {\rm g \ cm^{-2}}} \right)^{-1} \left(\frac{a_{\rm p}}{1 \ {\rm AU}} \right)^{1/2} \left(\frac{M_c}{M_\oplus} \right)^{1/3} \left(\frac{M_\star}{M_\odot} \right)^{-1/6} \times \left[\left(\frac{\Sigma_{\rm g}}{2400 \ {\rm g \ cm^{-2}}} \right)^{-2/5} \left(\frac{a_{\rm p}}{1 \ {\rm AU}} \right)^{2/20} \left(\frac{m}{10^{18} \ {\rm g}} \right)^{2/15} \right] \quad (10)$$

In this equation, $\Sigma_{\rm d}$ is the mean surface density of planetesimals in the planet feeding zone, while $\Sigma_{\rm g}$ is the gas surface density at the planet's position, m is the mass of the planetesimals, which is fixed to 10^{18} g, and $M_\oplus$ is the Earth mass. In the absence of orbital migration, solid cores can only grow to the isolation mass. This limit is set automatically in the code, since we calculate the corresponding decrease of the planetesimal surface density.

Once the gas disk has dissipated, the feeding zone increases as the protoplanet starts to increase its eccentricity. This allows solid planets to grow at a late time, but at a lower rate. The accretion timescale after the gas disk has dissipated is given as

$$\tau_{\rm c,nogas} = 2 \times 10^7 \ {\rm yr} \left(\frac{\Sigma_{\rm d}}{10 \ {\rm g \ cm^{-2}}} \right)^{-1} \left(\frac{a_{\rm p}}{1 \ {\rm AU}} \right)^{3/2} \left(\frac{M_c}{M_\oplus} \right)^{1/3} \left(\frac{M_\star}{M_\odot} \right)^{-1/2} \left(\frac{\rho_p}{1 \ {\rm g \ cm^{-3}}} \right)^{2/3}. \quad (11)$$

where we fix the planetary mean density in the simulation to 1 g/cm^3.

Both before and after the gas disk has dissipated, the core accretion rate is given as

$$\dot{M}_{\rm c} = \frac{M_{\rm c}}{\tau_{\rm c}}. \quad (12)$$

The core accretion rate can be scaled with the *CMdotc* parameter in the *paramsPFE.in* file to simulate the effects of a more rapid or slower accretion. When the planet has accreted also gas, $M_{\rm c}$ is replaced by $M_{\rm p}$, the total mass.

Figure 3 shows the result in a MMSN disk of numerically integrating Equation 12 using both Equation 10 and Equation 11. The growth is faster at smaller distances (growth wave propagating outward) as the collisional growth scales with the orbital frequency, but also it stops earlier, as the feeding zone and thus isolation mass is smaller close-in.

4. Accretion of gas

The accretion of nebular H/He onto the growing planet is modeled in a similar way as in Ida and Lin (2004), by considering the gas accretion timescale, and several criteria to terminate the growth.

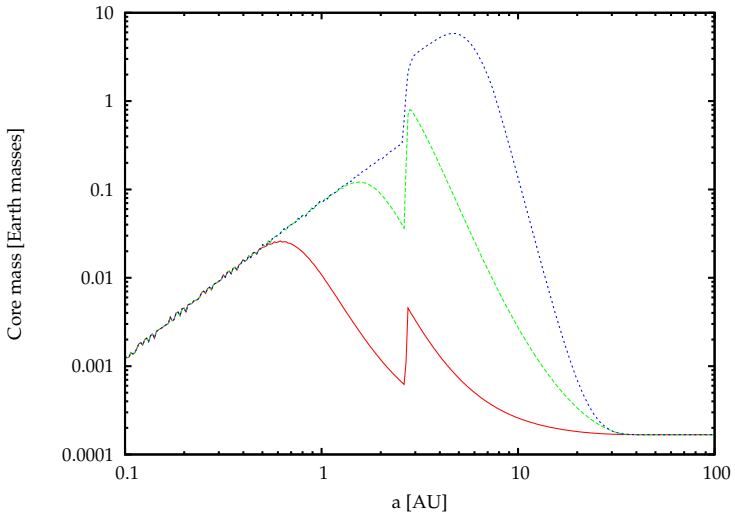

Fig. 3.— Core mass as a function of semi-major axis at 0.1 Myr (red), 1 Myr (green) and 10 Myr.

Gas accretion is assumed to start once the core mass exceeds the critical core mass that is calculated as

$$M_{\rm c,crit} = 10 M_\oplus \left(\frac{\dot{M}_{\rm c}}{10^{-6} M_\oplus \ {\rm yr}^{-1}} \right)^{1/4} \left(\frac{\kappa}{1 \ {\rm g \ cm}^{-2}} \right)^{1/4}. \tag{13}$$

where κ is the characteristic opacity in the protoplanetary atmosphere.

Then, the gas accretion rate is governed by the Kelvin-Helmholtz cooling timescale of the envelope, which is calculated as

$$\tau_{\rm KH} = 10^{p_{\rm KH}} \ {\rm yr} \left(\frac{M_{\rm p}}{M_\oplus} \right)^{q_{\rm KH}} \left(\frac{\kappa}{1 \ {\rm g \ cm}^{-2}} \right) \tag{14}$$

where $p_{\rm KH}$ and $q_{\rm KH}$ are parameters that are obtained by comparing the $\tau_{\rm KH}$ with internal structure calculations (Alibert et al. 2005). We use as nominal parameters the ones determined in Mordasini et al. (2014), $p_{\rm KH} = 10.4$ and $q_{\rm KH} = -1.5$, and $\kappa = 10^{-2}$ g/cm^2. These values ($p_{\rm KH}, q_{\rm KH}$, and κ) can be specified in the *paramsPFE.in* file. Gas accretion can be switched off by setting κ equal to a very large value (e.g. 10^{50} g/cm^2).

The gas accretion rate due to the contraction of the envelope is finally

$$\dot{M}_{\rm e,KH} = \frac{M_{\rm p}}{\tau_{\rm KH}}. \tag{15}$$

This gas accretion rate can be limited by several external effects. We assume that $\dot{M}_{\rm e}$ is limited by both the Bondi accretion rate (see Mordasini et al. 2012)

$$\dot{M}_{\rm e,Bondi} \approx \frac{\Sigma_{\rm g}}{H} \left(\frac{R_{\rm H}}{3} \right)^3 \Omega \tag{16}$$

and a fraction $f_{\rm lub99}$ of the viscous flux in the disk

$$\dot{M}_{\rm e,visc} = 3\pi\nu\Sigma_{\rm g} \tag{17}$$

where the viscosity is calculated as Shakura and Sunyaev (1973)

$$\nu = \alpha H^2 \Omega \tag{18}$$

and $f_{\rm lub99}$ is set to 0.9 (Lubow et al. 1999) meaning that the planet accretes 90% of the gas flow in the disk. The value of α can also be specified in the *paramPFE.in* file.

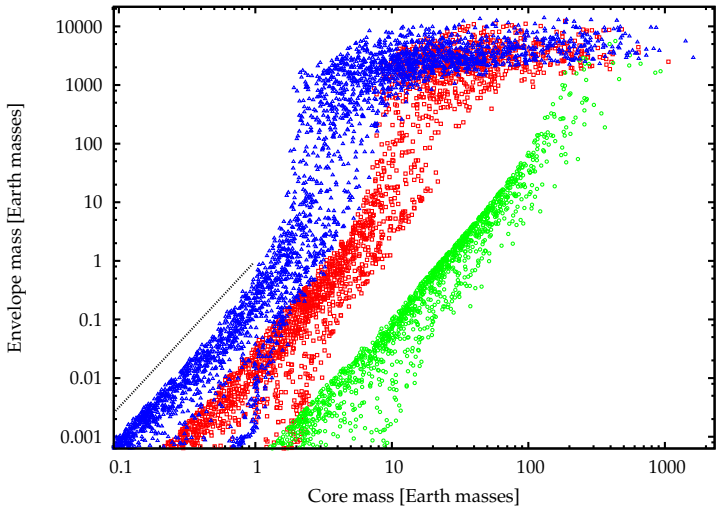

Fig. 4.— Envelope mass as a function of core mass at 10 Myrs for $\kappa = 10^{-3}$ (blue), 10^{-2} (red, nominal population, see below), and 1 (green) cm^2/g as found in population syntheses.

Figure 4 shows the envelope mass as a function of core mass for three different populations differing by κ. For lower κ, the higher $M_{\rm e}$ for a given core mass, as expected. At low masses, the envelope mass scales as $M_{\rm c}^{-q_{\rm KH}+1}$ (i.e. $M_{\rm c}^{2.5}$ in the simulation here, indicated by the black line, see Mordasini et al. 2014). Then, at a core mass of about 10 $M_\oplus$ (for the nominal case), gas accretion becomes efficient, and there are fewer planets in the intermediate mass range between about 10 to 100 $M_\oplus$. This is because the timescale to accrete this gas mass is clearly shorter than the disk lifetime, so that it is unlikely that the

disk disappears exactly at an intermediate moment/mass. This is the origin of the so called "planetary desert" (Ida and Lin 2004), which is typical for the core accretion mechanism. It is weaker in the model here due to the larger $q_{\rm KH} = -1.5$ instead of -3., meaning that the gas accretion rate does not as rapidly increase with mass, and due to the limits given by the Bondi and viscous accretion rate. At low opacity, giant planets already form for core masses as low as about 2 $M_\oplus$, while at the high, ISM like opacity, almost no giant planets form, because gas accretion takes too long compared to the disk lifetimes.

4.1. Truncation of gas accretion

We also need to specify at which mass the gas accretion is truncated. Five different possibilities are implemented:

1. Truncation at the gas isolation mass, assuming a feeding zone width for gas of 2 Hill spheres. The gas accretion rate is thus set to zero if the planet's envelope mass is higher than

$$M_{\rm iso,e} = \sqrt{\frac{(4\pi 2 a_{\rm p}^2 \Sigma_{\rm g})^3}{3 M_\star}}. \tag{19}$$

2. Truncation at the gap opening mass, assuming that gas accretion stops once the Hill sphere is larger than the disk's vertical scale height $R_{\rm H} > H$.

3. As in the last criterion, but if $R_{\rm H}$ is larger than 1.5 H, allowing for more massive planets.

4. No limitation, except when the planet has grown to a stellar mass ($\sim 0.1 M_\odot$)

5. A reduction (but not total truncation) of the gas accretion rate after gap formation, using the expression of Veras and Armitage (2004). The reduction factor of the gas accretion rate relative to the flux in the disk is given as

$$f_{\rm va04} = 1.668 \left(\frac{M_{\rm p}}{M_{\rm Jup}}\right)^{1/3} \exp\left(-\frac{M_{\rm p}}{1.5 M_{\rm Jup}}\right) + 0.04 \tag{20}$$

   and the gas accretion rate is

$$\dot{M}_{\rm e,va04} = f_{\rm va04} 3\pi\nu\Sigma_{\rm g}. \tag{21}$$

The last setting is the nominal case, but the criterion can be changed in the *paramsPFE.in* with the $ilimMe$ parameter.

5. Orbital migration

The gravitational interaction of the gaseous disk and the embedded protoplanet results in the exchange of angular momentum, which means that the planets change their semi-major axis due to migration (Goldreich and Tremaine 1979). Other effects (planetesimal driven migration, Kozai migration, planet-planet scattering) that can also modify the orbits are currently not implemented in the code.

The model includes both type I and type II migration. For both regimes, several prescriptions are implemented.

5.1. Type I migration

Type I migration is assumed to occur if the planet's Hill sphere radius is smaller than the disk's vertical scale height, i.e. for low-mass planets. The main ingredient for type I migration is the *torque*. To calculate the torque we need, among other quantities, the local power law exponent of the disk temperature $p_{\rm T}$ which is an input parameter of the model, and the local power law exponent of the gas surface density $p_{\rm g}$. This quantity is calculated numerically in the code. Three options for type I migration are implemented in the model:

1. Type I migration rate from Ida and Lin (2008). The migration timescale is given as

$$\tau_{\rm typeI} = \frac{1}{2.728 + 1.082 p_{\rm g}} \left(\frac{c_s}{a_{\rm p}\Omega}\right)^2 \frac{M_*}{M_{\rm p}} \frac{M_*}{a_{\rm p}^2 \Sigma_{\rm g}} \Omega^{-1} \tag{22}$$

   and the migration rate is

$$\dot{a}_{\rm p} = -\frac{a_{\rm p}}{\tau_{\rm typeI}} \tag{23}$$

2. Torque in a locally isothermal disk (Paardekooper et al. 2010). These authors found that the total torque in a locally isothermal regime, where the temperature T is constant in time but not with semi-major axis, is proportional to

$$\Gamma_{loc} = -0.85 + 0.9 p_{\rm T} + p_{\rm g}. \tag{24}$$

3. Torque in an adiabatic disk (Paardekooper et al. 2010). The Lindblad torque in an adiabatic disk is proportional to

$$\Gamma_{Lind} = \frac{1}{\gamma} \left(-2.5 + 1.7 p_{\rm T} - 0.1 p_{\rm g}\right) \tag{25}$$

while the corotation torque in the adiabatic case is proportional to

$$\Gamma_{Corot} = \frac{1}{\gamma}\left(1.65 + p_{\rm g}(9 - 7.9/\gamma) - 7.9 p_{\rm T}/\gamma\right) \tag{26}$$

where γ is the ratio of the heat capacities, fixed to 1.4 in the code (molecular hydrogen). The total torque due to the combination of the Lindblad and corotation torque finally is proportional to

$$\Gamma_{adia} = \Gamma_{Lind} + \Gamma_{Corot} \tag{27}$$

For the latter two cases, the final migration rate is then given as

$$\dot{a}_{\rm p} = \Gamma\ 2 a_{\rm p} \Omega \frac{a_{\rm p}^2}{h^2} \Sigma_{\rm g} \frac{M_{\rm p}}{M_*^2} \tag{28}$$

where $h = H/a_{\rm p}$ is the disk aspect ratio, and Γ is either Γ_{loc} or Γ_{adia}.

These migration rates can be scaled with the $C1$ parameter, and the description can be chosen with the *itypeI* parameter (1, 2, or 3) in the *paramsPFE.in* file. Type I migration can be switched off by setting $C1$=0.

5.2. Type II migration

Two options for type II migration are implemented in the model:

1. the type II migration rate as in Ida and Lin (2004) given as

$$\dot{a}_{\rm p} = 3\ {\rm sign}(a_{\rm p} - R_{\rm m}) \alpha \frac{\Sigma_{\rm g,m} R_{\rm m}^2}{M_{\rm p}} \frac{\Omega_{\rm m}}{\Omega} \left(\frac{H_{\rm m}}{a_{\rm p}}\right)^2 \Omega_{\rm m} \tag{29}$$

where quantities with the subscript m are evaluated at the radius of velocity reversal, i.e. where the disk changes from accreting to decreting (Lynden-Bell and Pringle 1974b)).

2. the type II migration rate as in Alibert et al. (2005), given as

$$\dot{a}_{\rm p} = {\rm sign}(a_{\rm p} - R_{\rm m})\ u_{\rm r}\ \min\left(1, \frac{2\Sigma_{\rm g} a_{\rm p}^2}{M_{\rm p}}\right) \tag{30}$$

where $u_{\rm r} = 3\nu/(2a_{\rm p})$ is the radial velocity of the accreting gas with $\nu = \alpha H^2 \Omega$, the turbulent viscosity.

The position of $R_{\rm m}$ is in both cases calculated as in Ida and Lin (2004)

$$R_{\rm m} = 10 \text{ AU} \exp\left(\frac{2t}{5\tau_{\rm disk}}\right). \tag{31}$$

These migration rates can be scaled with the $C2$ parameter, and the description can be chosen with the $itypeII$ parameter (1 or 2) in the *paramsPFE.in* file. Type II migration can be switched off by setting $C2$=0. The initial semi-major axis $a_{\rm p,init}$ of the embryo is another initial condition/Monte Carlo variable in the *globalPFE.in* file

Figure 5 shows the effect of (strongly reduced) type I and II migration in the nominal population. The plot shows that seeds with an initial orbital radius of about 1 AU can migrate very close to the star, while those starting at 10 AU can migrate to about 2 AU.

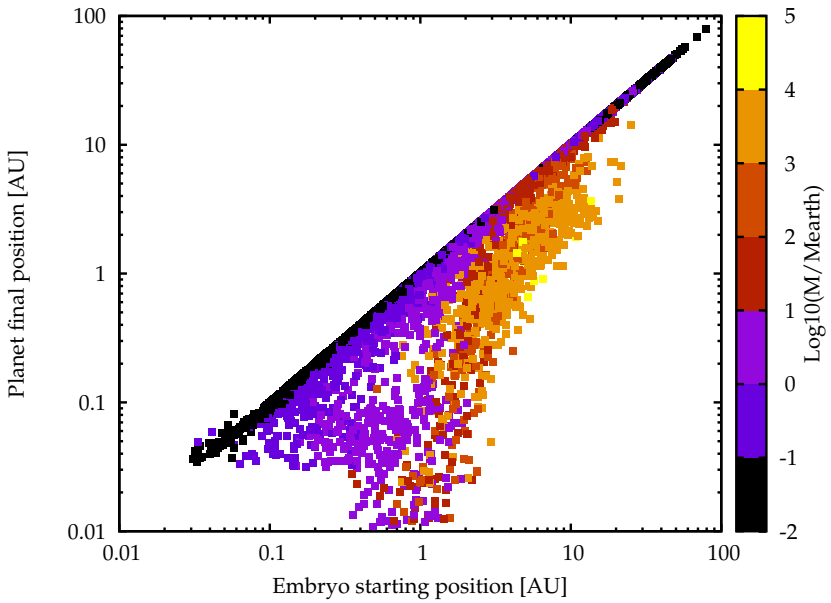

Fig. 5.— Relation of the initial embryo starting position and the final position of the planet in the nominal population. The colors give the planetary mass.

6. Probability distributions

The second crucial ingredients for a population synthesis model are sets of initial conditions (see Figure 1). These sets of initial conditions are drawn in a Monte Carlo way from probability distributions. These probability distributions represent the varying properties of protoplanetary discs and are derived as closely as possible from results of disc observations. Currently there are seven Monte Carlo variables, corresponding to the seven initial conditions in the *globalPFE.in* input file. They are:

1. The stellar mass
2. The inner disk radius (radius of the magnetospheric cavity)
3. The outer disk radius (start of exponential decrease)
4. The metallicity [Fe/H]
5. The disk gas mass scaling factor $f_{\rm g}$
6. The disk lifetime decay time
7. The initial starting position of the embryos

The way the generated distributions look like can be checked by looking at the *ref_red1e5.dat* file which contains the seven initial conditions and the values of the (nearly) initial disk gas and disk solid mass. As an illustration, Figure 6 shows scatter plots of the initial conditions for the nominal population.

The stellar mass is uniform in $\log(M_*)$ between 0.7 and 1.3 $M_\odot$ as in Ida and Lin (2004). The disk scaling factor $f_{\rm g}$ is lognormal distribution with a mean μ of $\log(f_{\rm g})$=0.25 dex, a dispersion σ of 0.5 dex, and a minimal $f_{\rm g}$=0.01 and a maximum of $f_{\rm g}$=10 (to avoid too massive, self-gravitationally unstable disks). [Fe/H] has a normal distribution with $\mu = -0.02$ and σ=0.22, as observed in solar like stars in the solar neighborhood (Mordasini et al. 2009b). Finally, the inner disk radius has a linear and uniform distribution between 0.01 and 0.03 AU, to mimic the effect of variable sizes of the magnetospheric cavity due to the observed spread of magnetic fields in T Tauri stars.

An important note: currently it is assumed that all distributions are independent from each other. It appears that in particular the disk mass or equivalently $f_{\rm g}$ scales with the stellar mass. It is simple to modify the code so that the mean value of the disk mass distribution scales with the stellar mass (e.g., approximately linearly, see Alibert et al. 2011).

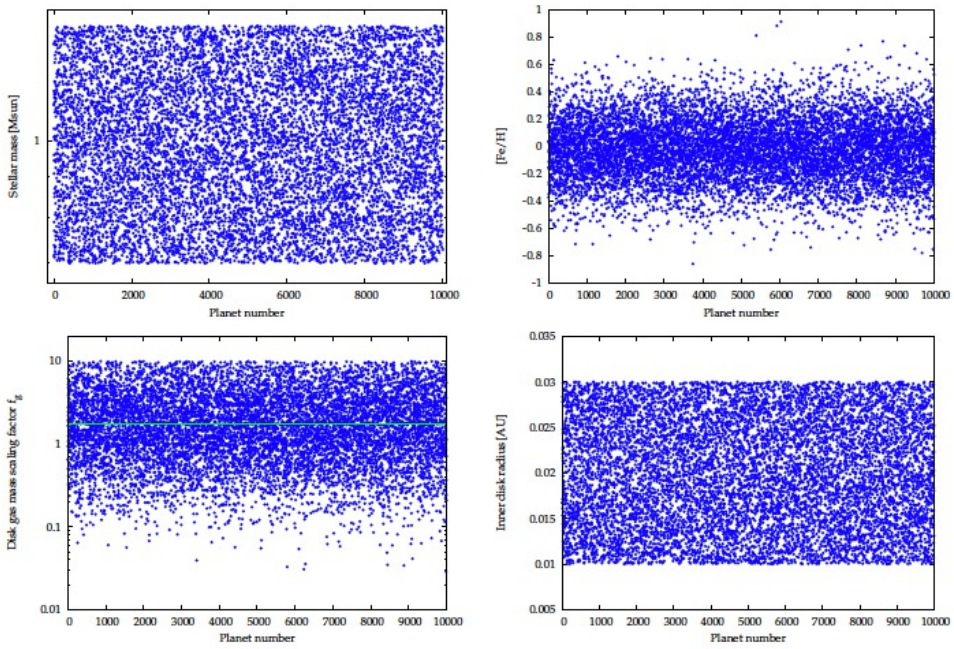

Fig. 6.— Distribution of some of the initial conditions in the nominal population.

7. Limitations

As a toy model, GlobalPFE has many limitations. The most important are:

- One embryo per disk: no dynamics, no competition for gas and solids, no eccentricity excitation, no capture in mean motion resonances ...
- Gas disk driven migration only (no scattering, no Kozai, no planetesimal driven migration)
- Core growth by accretion of planetesimals only, no pebble accretion
- Simplistic disk model (fixed temperature profile, no viscous evolution, no real photoevaporation model)
- Simplistic gas accretion model (no calculation of the envelope structure)
- No evolution of the disk of solid: no dust/planetesimal drift, growth, fragmentation, no eccentricity/inclination evolution
- No planetary internal structure and evolution: the planetary radius and luminosity are not calculated. The effect of atmospheric escape/envelope evaporation is also neglected.

REFERENCES

Y. Alibert, C. Mordasini, W. Benz, Extrasolar planet population synthesis. iii. formation of planets around stars of different masses. A&A **526**, 63 (2011)

Y. Alibert, C. Mordasini, W. Benz, C. Winisdoerffer, Models of giant planet formation with migration and disc evolution. A&A **434**, 343 (2005)

S.M. Andrews, D.J. Wilner, A.M. Hughes, C. Qi, C.P. Dullemond, Protoplanetary disk structures in ophiuchus. ii. extension to fainter sources. ApJ **723**, 1241 (2010)

W. Benz, S. Ida, Y. Alibert, D. Lin, C. Mordasini, Planet Population Synthesis. Protostars and Planets VI, 691–713 (2014)

K.-M. Dittkrist, C. Mordasini, H. Klahr, Y. Alibert, T. Henning, Impacts of planet migration models on planetary populations. Effects of saturation, cooling and stellar irradiation. A&A **567**, 121 (2014)

P. Goldreich, S. Tremaine, The excitation of density waves at the lindblad and corotation resonances by an external potential. ApJ **233**, 857 (1979)

S. Ida, D.N.C. Lin, Toward a deterministic model of planetary formation. i. a desert in the mass and semimajor axis distributions of extrasolar planets. ApJ **604**, 388 (2004)

S. Ida, D.N.C. Lin, Toward a deterministic model of planetary formation. iv. effects of type i migration. ApJ **673**, 487 (2008)

S.H. Lubow, M. Seibert, P. Artymowicz, Disk accretion onto high-mass planets. ApJ **526**, 1001 (1999)

D. Lynden-Bell, J.E. Pringle, The evolution of viscous discs and the origin of the nebular variables. MNRAS **168**, 603 (1974a)

D. Lynden-Bell, J.E. Pringle, The evolution of viscous discs and the origin of the nebular variables. MNRAS **168**, 603 (1974b)

C. Mordasini, P. Mollière, K.-M. Dittkrist, S. Jin, Y. Alibert, Global models of planet formation and evolution. International Journal of Astrobiology **14**, 201–232 (2015)

C. Mordasini, Y. Alibert, W. Benz, Extrasolar planet population synthesis. i. method, formation tracks, and mass-distance distribution. A&A **501**, 1139 (2009a)

C. Mordasini, Y. Alibert, W. Benz, D. Naef, Extrasolar planet population synthesis. ii. statistical comparison with observations. A&A **501**, 1161 (2009b)

C. Mordasini, Y. Alibert, H. Klahr, T. Henning, Characterization of exoplanets from their formation. i. models of combined planet formation and evolution. A&A **547**, 111 (2012)

C. Mordasini, H. Klahr, Y. Alibert, N. Miller, T. Henning A&A **566**, 141 (2014)

S.-J. Paardekooper, C. Baruteau, A. Crida, W. Kley, A torque formula for non-isothermal type i planetary migration - i. unsaturated horseshoe drag. MNRAS **401**, 1950 (2010)

J.B. Pollack, O. Hubickyj, P.H. Bodenheimer, J.J. Lissauer, M. Podolak, Y. Greenzweig, Formation of the giant planets by concurrent accretion of solids and gas. Icarus **124**, 62 (1996)

N.I. Shakura, R.A. Sunyaev, Black holes in binary systems. observational appearance. A&A **24**, 337 (1973)

E.W. Thommes, M.J. Duncan, H.F. Levison, Oligarchic growth of giant planets. Icarus **161**, 431 (2003)

D. Veras, P.J. Armitage, Outward migration of extrasolar planets to large orbital radii. MNRAS **347**, 613 (2004)